

# Microscopic Origin of Reduced Magnetic Order in a Frustrated Metal

X. Boraley,<sup>1</sup> O. Stockert,<sup>2,\*</sup> J. Lass,<sup>1</sup> R. Sibille,<sup>1</sup> Ø. S. Fjellvåg,<sup>1,3</sup>  
S. Moody,<sup>1</sup> A. M. Läuchli,<sup>4,5</sup> V. Fritsch,<sup>6</sup> and D. G. Mazzone<sup>1,†</sup>

<sup>1</sup>PSI Center for Neutron and Muon Sciences, 5232 Villigen PSI, Switzerland

<sup>2</sup>Max Plank Institute for Chemical Physics of Solids, DE 01187 Dresden, Germany

<sup>3</sup>Department for Hydrogen Technology, Institute for Energy Technology, PO Box 40, NO-2027, Kjeller, Norway

<sup>4</sup>PSI Center for Scientific Computing, Theory and Data, 5232 Villigen PSI, Switzerland

<sup>5</sup>Institute of Physics, École Polytechnique Fédérale de Lausanne (EPFL), 1015 Lausanne, Switzerland

<sup>6</sup>Experimental Physics VI, Center for Electronic Correlations and Magnetism,  
Institute of Physics, University of Augsburg, 86135 Augsburg, Germany

(Dated: February 14, 2025)

Although magnetic frustration in metals provides a promising avenue for novel quantum phenomena, their microscopic interpretation is often challenging. Here we use the face-centered cubic intermetallic HoInCu<sub>4</sub> as model material to show that Hamiltonians neglecting the charge degree of freedom are appropriate for frustrated metals possessing low density of states at the Fermi surface. Through neutron scattering techniques we determine matching magnetic exchange interactions in the paramagnetic and field-polarized states using an effective spin-1 Heisenberg Hamiltonian, for which we identify antiferromagnetic nearest and next-nearest neighbour interactions  $J_1$  and  $J_2$  that are close to the critical ratio  $J_2/J_1 = 1/2$ . The study further provides evidence that spin-wave theory fails to predict the low-energy spin dynamics in the antiferromagnetic zero-field state, which is dominated by overdamped magnetic excitations. We conclude that the low-energy fluctuations arise from quantum fluctuations, accounting for the missing moment of the strongly renormalized magnetic long-range order.

Magnetic frustration arises in materials in which the magnetic interactions cannot be minimized simultaneously due to constraints of the underlying lattice geometry or because of conflicting exchange interactions. The resulting degeneracy between frustrated ground-state configurations can lead to strong fluctuations triggering unconventional phases of matter, such as (quantum) spin liquids and other exotic spin states that are of fundamental and technological interest [1–7]. Progress in the microscopic understanding of these exotic magnetic states is frequently achieved through theoretical models, in which Heisenberg, Ising or Kitaev Hamiltonians are used to treat the nearest-neighbour magnetic interactions [2, 8]. These models are particularly successful in describing insulating materials, where further-neighbour interactions decay exponentially with distance and higher-order spin interactions are weak. In contrast, less research has been conducted on itinerant materials [4, 6], mainly because the dominating contribution of the charge degree of freedom leads to additional challenges. Magnetic exchange interactions in metals typically originate from couplings of the conduction electrons with local moments [9–12], which can trigger anisotropic exchanges, strong further-neighbour and higher-order exchange interactions. These contributions can either lift the degeneracy of magnetic ground states or trigger novel quantum phases in metals [6, 7, 9, 13] whose interpretation are often challenging. In metals containing Ce, Eu, Sm or Yb, the situation is further complicated, because favorable

oxidation states allow for a finite Kondo exchange coupling that screens the local moments [14]. This makes it difficult to unambiguously distinguish effects invoked by the Kondo process from magnetic frustration.

Progress in our microscopic understanding of how magnetic frustration is established in itinerant materials can be gained with a stepwise approach, in which we focus first on metals with only minor contributions of the charge degree of freedom and without Kondo screening. In this Letter, the intermetallic compound HoInCu<sub>4</sub> serves as representative example. Holmium features a stable +3 oxidation state, and the electronic density of states at the Fermi surface in HoInCu<sub>4</sub> is strongly reduced [15]. The material crystallizes in a face-centered cubic lattice structure ( $a = 7.178$  Å) that is prone to frustration [16–26]. This has been confirmed through a low Néel temperature  $T_N = 0.76$  K at which only a fraction of the magnetic entropy is released and recovered solely at significantly higher temperature [15]. Below  $T_N$  magnetic long-range order is established in a type-III antiferromagnetic (AFM) structure (see Fig. 1a) with propagation vector  $\vec{q} = (1, \frac{1}{2}, 0)$  in reciprocal lattice units (rlu). Intriguingly, the ordered magnetic moment refined by neutron powder diffraction is significantly lower than the ordered moment expected from the crystal-field ground state triplet [15]. These findings led to the proposal that HoInCu<sub>4</sub> hosts a partially long-range ordered ground state [15].

Here we study the microscopic origin of the magnetic ground state. We unambiguously determine the nearest and next-nearest neighbour interactions through neutron diffraction and inelastic neutron scattering in the paramagnetic ( $T > T_N$ ,  $\mu_0 H = 0$  T) and field-polarized ( $T \sim 0$

\* oliver.stockert@cpfs.mpg.de

† daniel.mazzone@psi.ch

$K, H > H_c$ ) states, respectively. These results are used to discuss the nature of the antiferromagnetic state, for which we observe overdamped excitations. We find that they arise from quantum fluctuations that lead to moment fluctuations down to lowest temperatures within a magnetic long-range ordered state possessing a strongly reduced ordered moment.

The study was conducted on the same well-characterised HoInCu<sub>4</sub> single crystal as in Ref. [15]. The  $m = 630$  mg sample was aligned perpendicular to the  $c$ -axis, yielding a horizontal  $(H, K, 0)$ -scattering plane in all neutron scattering experiments. The diffraction studies were performed on the thermal and cold diffractometers ZEBRA and DMC at the Paul Scherrer Institut (PSI), Switzerland [27]. On ZEBRA we used an incoming neutron wavelength of  $\lambda = 1.383$  Å. The sample was cooled to temperatures below  $T = 0.1$  K employing a cryostat with dilution insert. Reciprocal space maps were taken with sample rotation steps of 0.125 degree, and recorded with a position sensitive area detector. The background was measured in two datasets at  $T = 50$  and 100 K, which were combined for the data analysis. The background-subtracted diffuse neutron scattering signal was analyzed with the Spinteract software package [28]. An incoming wavelength  $\lambda = 4.5189$  Å was used for the experiments on DMC, using either dilution or <sup>3</sup>He inserts. The zero-field data of these two experiments were combined by accounting for intensity differences and systematic temperature shifts through overlapping data points. The field dependence of the magnetic signal was studied in a vertical 10 T-cryomagnet at fields from  $\mu_0 H = 0$  to 5 T with  $H \parallel [0, 0, 1]$ . In all experiments at DMC, the background was determined at  $T = 50$  K. The inelastic neutron scattering experiment was performed on the multiplexing spectrometer CAMEA at PSI using a dilution insert in a vertical 11 T-cryomagnet to reach a base temperature of  $T = 40$  mK [29, 30]. Excitation spectra were recorded with one degree sample rotation steps with energy transfers  $E = 0 - 7$  meV. We used incident energies  $E_i = 3.38$  and 4.04 meV yielding an elastic resolution of 100  $\mu$ eV full width at half maximum (FWHM) to study the low-energy zero-field excitations ( $E < 0.9$  meV) of the material. For these data a background was taken at  $\mu_0 H = 10$  T for which the region  $E < 0.9$  meV did not contain any magnetic fluctuations. An  $E_i = 5$  meV was used for the scans under magnetic field, resulting in a FWHM of 180  $\mu$ eV and  $E < 2$  meV. Spin-wave calculations were performed through the Su(n)ny and SpinW software packages [31, 32]. Measurements up to  $E = 7$  meV were recorded to determine the crystal-electric field scheme at zero field and were analyzed with PyCrystalField [33]. The refined values from our single crystal inelastic neutron scattering experiment match those obtained from powder samples (see Ref. [15] and Supplemental Material (SM) Note 1). They show that the crystal-field ground state is a triplet, justifying the approximation of an effective spin-1 Hamiltonian at low temperature.

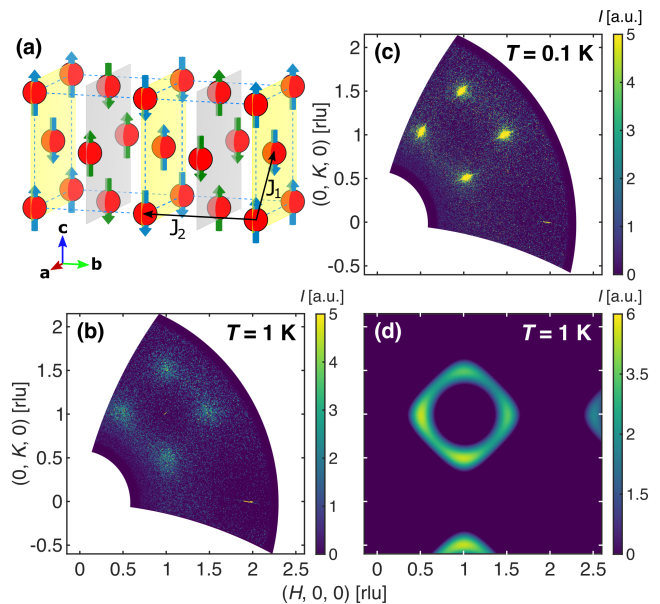


FIG. 1. (a) Illustration of the type-III antiferromagnetic (AFM) structure. The propagation vector  $\vec{q} = (1, \frac{1}{2}, 0)$  in reciprocal lattice units (rlu) splits the face-centered cubic lattice into two independent sublattices, which are indicated with yellow and gray sheets. The magnetic moments corresponding to each sublattice are shown with blue and green arrows.  $J_1$  and  $J_2$  indicate the magnetic nearest and next-nearest neighbour exchange interactions. (b) and (c) Colour-coded background subtracted diffraction maps of HoInCu<sub>4</sub> in the  $(H, K, 0)$ -plane measured at temperatures above and below the Néel temperature  $T_N = 0.76$  K. The colour bar represents the neutron intensity  $I$ . (d) Simulated magnetic diffraction pattern at  $T = 1$  K obtained with the refined parameters  $J_1 = 0.64(6)$  K and  $J_2 = 0.29(2)$  K.

Figures 1b and c depict colour-coded single-crystal diffraction maps in the  $(H, K, 0)$ -plane measured on ZEBRA at zero-field and  $T = 1$  and 0.1 K, respectively. Above  $T_N = 0.76$  K the data reveal a diffuse magnetic signal at reciprocal lattice positions with  $\vec{q} = (1, \frac{1}{2}, 0)$ , in agreement with the predicted paramagnetic susceptibility of the type-III AFM order [26]. At  $T = 0.1$  K  $< T_N$  sharp magnetic Bragg peaks appear at the same wavevectors, but are surrounded by a diffuse signal. The scattering signal was fitted to a combination of two-dimensional Gaussian and Lorentzian lineshapes. Two Gaussian widths account for the axial instrument resolution that leads to an elongated shape of the magnetic Bragg peaks. The diffuse signal was fitted to two-dimensional Lorentzians with a single width, because the inherently broad signal substantially exceeds the instrument resolution.

The temperature dependence of the integrated intensities and correlation lengths ( $\xi = \frac{a}{\pi \text{FWHM}}$ ) is presented in Fig. 2a and b. The temperature-dependent integrated intensity shows that the magnetic diffuse signal has an onset above  $T_N$  and is continuously increasing as the temperature decreases. This trend is persistent even deep in-

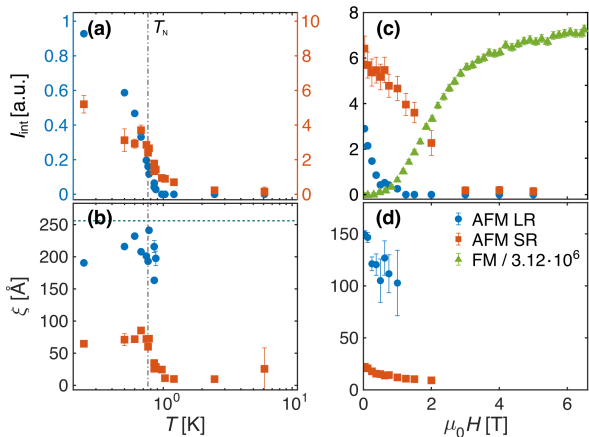


FIG. 2. Integrated intensity  $I_{int}$  and correlation lengths  $\xi = \frac{\alpha}{\pi \text{FWHM}}$  of the AFM long- (LR) and short-range (SR) orders as function of temperature (a, b) and magnetic field (c, d). The field dependence measured at  $T = 0.1$  K (measured at DMC) is plotted together with the ferromagnetic (FM) contribution to the structural  $(2, 0, 0)$  Bragg peak at  $T = 0.04$  K (measured at CAMEA).

side the long-range ordered phase. The temperature dependence of the correlation lengths shows that the diffuse short-range order is correlated over roughly 10 unit cells below  $T_N$ , while the magnetic long-range order is correlated over 31 unit cells. The latter value is slightly below the instrument resolution (see dashed line in Fig. 2b), which likely results from finite magnetic domain sizes.

The magnetic short-range correlations above  $T_N$  hold information on the magnetic exchange interactions in the material. Since the metal possesses a low electronic density of states at the Fermi surface [15], we approximate the material with a localized system similar to a magnetic insulator. We consider a nearest ( $J_1$ ) and next-nearest ( $J_2$ ) neighbour Heisenberg Hamiltonian with

$$\mathcal{H}_{\text{AFM}} = J_1 \sum_{\langle i, j \rangle} \vec{S}_i \cdot \vec{S}_j + J_2 \sum_{\langle\langle i, j \rangle\rangle} \vec{S}_i \cdot \vec{S}_j \quad (1)$$

Here,  $\langle i, j \rangle$  and  $\langle\langle i, j \rangle\rangle$  uniquely assigns all nearest and next-nearest neighbour bonds, respectively, and  $\vec{S}_i$  is a  $S = 1$  spin operator at site  $i$ . Our analysis yields antiferromagnetic exchange interactions  $J_1 = 0.64(6)$  K and  $J_2 = 0.29(2)$  K (see Fig. 1d and SM Note 2 for further details). The resulting  $J_2/J_1 = 0.45(5)$  ratio is compatible with the observed type-III AFM order predicted for  $0 < J_2/J_1 < 0.5$  [20, 21]. Notably, our results classify HoInCu<sub>4</sub> as a rare type-III AFM case close to the type-II AFM phase boundary with  $\vec{q} = (\frac{1}{2}, \frac{1}{2}, \frac{1}{2})$  predicted for  $J_2/J_1 \geq 0.5$  [18, 20, 21].

Figures 2c and d show the magnetic field dependence of the magnetic long- and short-range orders for  $H || [0, 0, 1]$  and  $T = 0.1$  K. The results stem from one-dimensional Gaussian and Lorentzian fits to reciprocal space maps recorded on DMC. We observe that the integrated mag-

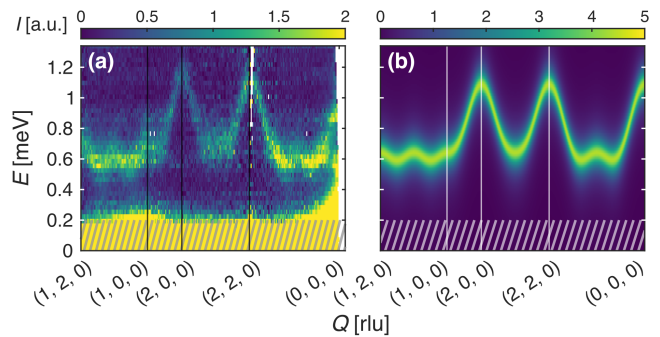


FIG. 3. (a) Spin-wave spectrum of HoInCu<sub>4</sub> at  $\mu_0 H = 5$  T and  $T = 40$  mK for a representative path through the  $(H, K, 0)$ -plane. An integration width of  $\Delta Q = 0.35$  rlu perpendicular to the cut was used. (b) Linear spin-wave simulation obtained with the refined parameters  $J_1 = 0.66(3)$  K and  $J_2 = 0.30(3)$  K. A Lorentzian smearing  $\Delta E = 0.08$  meV half width half maximum was used to mimic the instrument resolution. The hashed region at low energy transfers  $E$  represents the elastic line resolution.

netic Bragg intensity corresponding to the AFM long-range order is suppressed above  $\mu_0 H \approx 1$  T. In contrast the short-range correlations survive to larger magnetic fields of  $\mu_0 H \approx 2.5$  T, revealing a field range between  $\mu_0 H \approx 1$  and 2.5 T in which only short-range correlations are present. The magnetization of the material was probed via the ferromagnetic (FM) contribution to the structural  $(2, 0, 0)$  Bragg peak intensity at  $T = 40$  mK on CAMEA, supporting that the field-polarized state is reached above  $\mu_0 H > \mu_0 H_c = 2.5$  T.

The field-polarized state serves as an alternative way to determine the magnetic interaction parameters, as in this regime linear spin-wave theory is known to be exact. Figure 3a shows the field-polarized excitation spectrum at  $\mu_0 H = 5$  T along a representative path in the  $(H, K, 0)$ -plane. The spectrum was measured at  $T = 40$  mK on CAMEA. The field-polarized excitation spectra were analyzed using the same spin-1 Hamiltonian as in Eq. 1 with an additional Zeeman term accounting for the magnetic field anisotropy.

$$\mathcal{H}_{\text{FP}} = \mathcal{H}_{\text{AFM}} - g\mu_B\mu_0 H \sum_i S_i^z \quad (2)$$

The effective  $g$ -factors at  $\mu_0 H = 4, 5$  and 6.5 T were determined from the polarized spin-wave maxima and compared with the predicted field evolution of the crystal-field ground state triplet. We found that the linear Zeeman term is only approximate for the crystal-field scheme of HoInCu<sub>4</sub>. Thus, a field dependent  $g$ -factor was assumed for the effective spin-1 treatment, and note that more accurate results can be obtained if all crystal-field wave-functions are considered in the spin-wave analysis (see SM Note 3 for details). Within the effective spin-1 treatment refinements over 820 data points yield  $J_1 = 0.66(3)$  K and  $J_2 = 0.30(3)$  K, which is in agreement with

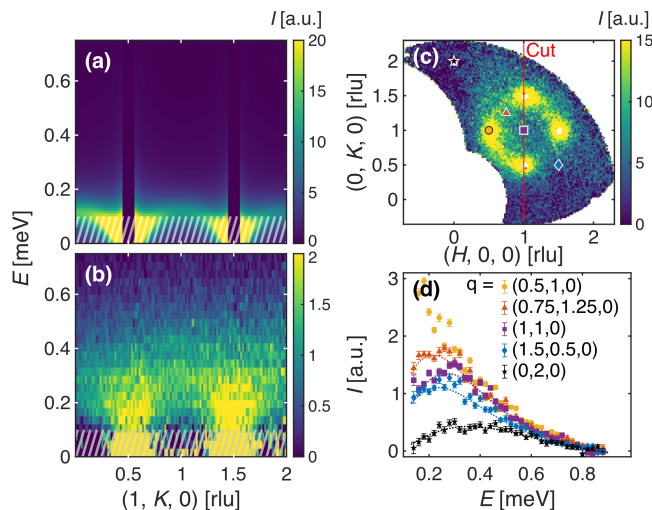


FIG. 4. (a) Linear spin-wave simulation of the type-III AFM state along  $(1, K, 0)$ . The divergence occurring at the magnetic positions has been removed for clarity. The instrument resolution was approximated with a Lorentzian smearing  $\Delta E = 0.04$  meV half width half maximum. (b) Background subtracted magnetic excitation spectrum along  $(1, K, 0)$ , using an integration width  $\Delta Q = 0.35$  rlu perpendicular to the cut (c) Reciprocal space map at an energy transfer  $E = 0.00(5)$  meV. The intensity at the magnetic magnetic Bragg peaks have been removed for clarity. The cut indicated in the panel represents the path plotted in panel (b). (d) Energy cuts at the reciprocal space positions indicated in panel (c), with circular integration width  $\Delta Q = 0.2$  rlu. The data are overplotted with damped harmonic oscillator fits, revealing a relaxation rate of  $\sim 4J_1$ .

our analysis of the magnetic correlations above  $T_N$ . The corresponding linear spin-wave simulation at  $\mu_0 H = 5$  T is plotted in Fig. 3b.

Having determined matching interaction parameters in the paramagnetic and field-polarized states, we expect these parameters will also be applicable in the type-III AFM ground state. Using linear spin-wave theory magnetic excitations are expected below an energy transfer  $E = 0.2$  meV (see Fig. 4a). The observed magnetic excitation spectrum at  $T = 40$  mK is displayed in Fig. 4b (see also SM Note 4 for further cuts and simulations). Their comparison provides evidence that linear spin-wave theory fails to capture the low-energy spin dynamics in  $\text{HoInCu}_4$ . In contrast to the predictions we observe column-like excitations centered around the magnetic Bragg peak positions. The excitations are most intense around  $E \approx 0.3$  meV and display only a weak momentum dependence. The life-time of the damped excitations was assessed through one-dimensional energy cuts at specific reciprocal lattice positions indicated in Fig. 4c, showing a thin slice ( $E = 0.00(5)$  meV) around the elastic  $(H, K, 0)$ -plane. The resulting cuts shown in Fig. 4d were fitted to a damped harmonic oscillator, for which we find a global relaxation rate  $\Gamma = 0.24(2)$  meV corresponding to roughly  $\sim 4J_1$ .

Figure 4c reveals a broad elastic intensity distribution that is centered around the magnetic Bragg peaks and shows some finite intensity along the shortest path connecting neighbouring peaks. This result provides evidence that within our resolution of 0.1 meV, a substantial fraction of the Ho moments remain short-range correlated. We estimated the fluctuating moment fraction through a refinement of the diffuse scattering signal that was measured below  $T_N$  during the diffraction experiment on ZEBRA (see Fig. 1c), using the interaction parameters obtained from the analysis of the paramagnetic state (see SM Note 2 for details). The results are in agreement with the experimental observations, if about 30% of the Ho moment remains fluctuating within the long-range ordered state.

A strong renormalization of the ordered magnetic moment together with complex dynamic many-body properties is a trait mark of quantum effects in frustrated magnets [1–3, 20–24, 34, 35]. While frustrated triangular and square lattices are prime geometries for quantum effects to appear [34, 35], an increasing amount of theoretical studies have found that quantum fluctuations are also important in face-centered cubic lattices [20–24]. For instance, it is predicted that the type-III AFM state is unstable at the phase boundaries  $J_2/J_1 = 0$  and 0.5, but that thermal fluctuations can help to stabilize the structure [20, 21, 23]. While such an order-by-disorder transition has been recently observed in  $\text{K}_2\text{IrCl}_6$  close to  $J_2/J_1 = 0$  [36], the inaccessibility of materials close to  $J_2/J_1 = 0.5$  hitherto hindered experimental studies to the type-II/type-III AFM phase boundary.  $\text{HoInCu}_4$  bridges this issue, because our results provide compelling evidence that the material can be modeled as an effective spin-1 Heisenberg system with  $J_2/J_1 = 0.45(5)$ . The importance of quantum fluctuations was assessed using spin-wave theory including quantum corrections of the leading term in  $1/S$ . We obtain that the expected ordered moment of  $\text{HoInCu}_4$  is renormalized by about 30%, which matches the estimated fluctuating moment fraction. These results are also in agreement with previous results reporting a mismatch between the ordered moment expected from the crystal-field ground state triplet ( $\mu_{CEF} = 4.58\mu_B$ ), and the magnetic moment ( $\mu = 3.23(4)\mu_B$ ) refined from neutron powder diffraction [15]. Thus, our results provide evidence for the presence of substantial quantum fluctuations, accounting for the missing moment of the renormalized magnetic long-range order.

We note that neutron scattering can a priori not discriminate a case in which the ordered moment is homogeneously reduced, from a spatially inhomogeneous scenario in which half of the Ho ions carry the full moment and the other half remain disordered (see also SM Note 4). The latter case is enabled through the ordering wavevector  $\vec{q} = (1, \frac{1}{2}, 0)$ , splitting the face-centered cubic type-III AFM structure into two orbits with independent Ho sublattices (see Fig. 1a) [15, 19, 37, 38]. While modern theoretical considerations of frustrated magnets favor

homogeneous solutions [20, 34, 35], local probes such as muon spin rotation and nuclear spin resonance or neutron diffraction under uniaxial pressure may be able to experimentally distinguish the two scenarios. We further mention that HoInCu<sub>4</sub> potentially hosts an intriguing quantum phase between  $\mu_0 H \approx 1$  and 2.5 T, at which magnetic long-range order is suppressed but short-range correlations are still present. In fact, linear spin-wave theory predicts the critical field around  $\mu_0 H_c \approx 2.5$  T (see SM Note 5), but fails to capture the nature of the magnetic state in this field range. Future theoretical and experimental efforts are required to elucidate the microscopic nature of this phase.

Finally, we claim that the reported study has an impact beyond the field of frustrated magnetism in face-centered cubic lattices. Although magnetic frustration is often challenging to interpret in metals, we here show that progress in the microscopic understanding of frustrated Fermi liquids can be gained with a step-wise approach. We elucidate that local Hamiltonians neglecting the charge degree of freedom provide an appropriate description of frustrated magnetic properties in metals possessing low-density of states at the Fermi surface. We hypothesize that such studies can build a foundation to

gain insight in how magnetic frustration is established in metals, in which the charge degree of freedom plays a more significant role.

In summary, we have studied the microscopic origin of the magnetic ground state in metallic HoInCu<sub>4</sub> possessing only minor contribution of the charge degree of freedom at the Fermi level. Using an effective spin-1 Heisenberg Hamiltonian we find matching nearest and next-nearest neighbour exchange couplings in the paramagnetic and magnetic field-polarized states. The resulting  $J_2/J_1 = 0.45(5)$  ratio is compatible with theoretical models for face-centered cubic lattices, identifying the material as a rare type-III AFM close to the phase boundary  $J_2/J_1 = 0.5$  [18, 20, 21]. In contrast to classical predictions we find a non-trivial type-III AFM state with an overdamped magnon spectrum below  $T_N$  and at zero magnetic field. Our investigations provide evidence that the low-energy fluctuations arise from quantum fluctuations, accounting for the missing moment of the renormalized ordered moment value in the AFM ground state.

We thank Joseph Paddison and Oksana Zaharko for fruitful discussions. We acknowledge the Paul Scherrer Institut for the allocated beam time on ZEBRA, DMC and CAMEA, alongside the Swiss National Foundation for financial support (Grant No. 200021.200653).

- 
- [1] L. Balents, Spin liquids in frustrated magnets, *Nature* **464**, 199 (2010).
- [2] C. Broholm, R. Cava, S. Kivelson, D. Nocera, M. Norman, and T. Senthil, Quantum spin liquids, *Science* **367**, eaay0668 (2020).
- [3] Y. Zhou, K. Kanoda, and T.-K. Ng, Quantum spin liquid states, *Rev. Mod. Phys.* **89**, 025003 (2017).
- [4] M. Vojta, Frustration and quantum criticality, *Reports on Progress in Physics* **81**, 064501 (2018).
- [5] K. Plumb, H. Changlani, A. Scheie, S. Zhang, J. Kriza, J. Rodriguez Rivera, Y. Qiu, B. Winn, R. Cava, and C. Broholm, Continuum of quantum fluctuations in a three-dimensional  $s = 1$  heisenberg magnet, *Nature Physics* **15**, 54 (2019).
- [6] C. Lacroix, Frustrated metallic systems: A review of some peculiar behavior, *Journal of The Physical Society of Japan - J PHYS SOC JPN* **79** (2010).
- [7] S. Gao, O. Zaharko, V. Tsurkan, Y. Su, J. S. White, G. S. Tucker, B. Roessli, F. Bourdarot, R. Sibille, D. Chernyshov, T. Fennell, A. Loidl, and C. Rüegg, Spiral spin-liquid and the emergence of a vortex-like state in mnsc2s4, *Nature Physics* **13**, 157 (2017).
- [8] O. A. Starykh, Unusual ordered phases of highly frustrated magnets: a review, *Reports on Progress in Physics* **78**, 052502 (2015).
- [9] S. Hayami and Y. Motome, Topological spin crystals by itinerant frustration, *Journal of Physics: Condensed Matter* **33**, 443001 (2021).
- [10] M. A. Ruderman and C. Kittel, Indirect exchange coupling of nuclear magnetic moments by conduction electrons, *Phys. Rev.* **96**, 99 (1954).
- [11] T. Kasuya, A Theory of Metallic Ferromagnetism and Antiferromagnetism on Zener's Model, *Progress of Theoretical Physics* **16**, 45 (1956), <https://academic.oup.com/ptp/article-pdf/16/1/45/5266722/16-1-45.pdf>.
- [12] K. Yosida, Magnetic properties of cu-mn alloys, *Phys. Rev.* **106**, 893 (1957).
- [13] T. Kurumaji, T. Nakajima, M. Hirschberger, A. Kikkawa, Y. Yamasaki, H. Sagayama, H. Nakao, Y. Taguchi, T. hisa Arima, and Y. Tokura, Skyrmion lattice with a giant topological hall effect in a frustrated triangular-lattice magnet, *Science* **365**, 914 (2019), <https://www.science.org/doi/pdf/10.1126/science.aau0968>.
- [14] J. Kondo, Resistance Minimum in Dilute Magnetic Alloys, *Progress of Theoretical Physics* **32**, 37 (1964), <https://academic.oup.com/ptp/article-pdf/32/1/37/5193092/32-1-37.pdf>.
- [15] O. Stockert, J.-U. Hoffmann, M. Mühlbauer, A. Senyshyn, M. M. Koza, A. A. Tsirlin, F. M. Wolf, S. Bachus, P. Gegenwart, R. Movshovich, S. Bobev, and V. Fritsch, Magnetic frustration in a metallic fcc lattice, *Phys. Rev. Res.* **2**, 013183 (2020).
- [16] T. Chatterji, L. P. Regnault, S. Ghosh, and A. Singh, Magnetic excitations in frustrated fcc type-iii antiferromagnet mns2, *Journal of Physics: Condensed Matter* **31**, 125802 (2019).
- [17] M. Matsuura, Y. Endoh, H. Hiraka, K. Yamada, A. S. Mishchenko, N. Nagaosa, and I. V. Solovyev, Classical and quantum spin dynamics in the fcc antiferromagnet nis<sub>2</sub> with frustration, *Phys. Rev. B* **68**, 094409 (2003).
- [18] D. C. Joshi, P. Pramanik, S. Nayak, K. Dasari, R. J. Choudhary, and S. Thota, Magnetic exchange interactions and dielectric studies of zn1-x nix-nio composites,

- Journal of Physics D: Applied Physics* **50**, 325002 (2017).
- [19] H. Nakamura, N. Kim, M. Shiga, R. Kmieć, K. Tomala, E. Ressouche, J. P. Sanchez, and B. Malaman, the partially disordered state of the frustrated face-centred cubic antiferromagnet, *Journal of Physics: Condensed Matter* **11**, 1095 (1999).
- [20] J. Oitmaa, Ordered phases in the frustrated fcc lattice antiferromagnet, *Phys. Rev. B* **108**, 014414 (2023).
- [21] N.-N. Sun and H.-Y. Wang, The j1-j2 model on the face-centered-cubic lattices, *Journal of Magnetism and Magnetic Materials* **454**, 176 (2018).
- [22] T. Yildirim, A. B. Harris, and E. F. Shender, Frustration and quantum fluctuations in heisenberg fcc antiferromagnets, *Phys. Rev. B* **58**, 3144 (1998).
- [23] R. Schick, O. Götze, T. Ziman, R. Zinke, J. Richter, and M. E. Zhitomirsky, Ground-state selection by magnon interactions in a fcc antiferromagnet, *Phys. Rev. B* **106**, 094431 (2022).
- [24] R. Schick, T. Ziman, and M. E. Zhitomirsky, Quantum versus thermal fluctuations in the fcc antiferromagnet: Alternative routes to order by disorder, *Phys. Rev. B* **102**, 220405 (2020).
- [25] L. Batalov and A. Syromyatnikov, Order-by-disorder effects in antiferromagnets on face-centered cubic lattice, *Journal of Magnetism and Magnetic Materials* **414**, 180 (2016).
- [26] D. Kiese, T. Müller, Y. Iqbal, R. Thomale, and S. Trebst, Multiloop functional renormalization group approach to quantum spin systems, *Phys. Rev. Res.* **4**, 023185 (2022).
- [27] J. Lass, S. H. Moody, and Øystein Slagtern Fjellvåg, *Dmcpv: A powder and single crystal neutron diffraction software for dmc* (2025), [arXiv:2501.08845](https://arxiv.org/abs/2501.08845) [physics.data-an].
- [28] J. A. M. Paddison, Spinteract: a program to refine magnetic interactions to diffuse scattering data, *Journal of Physics: Condensed Matter* **35**, 495802 (2023).
- [29] J. Lass, H. Jacobsen, K. M. L. Krighaar, D. Graf, F. Groitl, F. Herzog, M. Yamada, C. Kägi, R. A. Müller, R. Bürge, M. Schild, M. S. Lehmann, A. Bollhalder, P. Keller, M. Bartkowiak, U. Filges, U. Greuter, G. Theidel, H. M. Rønnow, C. Niedermayer, and D. G. Mazzone, Commissioning of the novel Continuous Angle Multi-energy Analysis spectrometer at the Paul Scherrer Institut, *Review of Scientific Instruments* **94**, 023302 (2023), <https://pubs.aip.org/aip/rsi/article-pdf/doi/10.1063/5.0128226/16681814/023302.1.online.pdf>.
- [30] J. Lass, H. Jacobsen, D. G. Mazzone, and K. Lefmann, Mjolnir: A software package for multiplexing neutron spectrometers, *SoftwareX* **12**, 100600 (2020).
- [31] D. Dahlbom, H. Zhang, C. Miles, S. Quinn, A. Niraula, B. Thipe, M. Wilson, S. Matin, H. Mankad, S. Hahn, D. Pajerowski, S. Johnston, Z. Wang, H. Lane, Y. W. Li, X. Bai, M. Mourigal, C. D. Batista, and K. Barros, *Sunny.jl: A julia package for spin dynamics* (2025), [arXiv:2501.13095](https://arxiv.org/abs/2501.13095) [quant-ph].
- [32] S. Toth and B. Lake, Linear spin wave theory for single-q incommensurate magnetic structures, *Journal of Physics: Condensed Matter* **27**, 166002 (2015).
- [33] A. Scheie, *PyCrystalField*: software for calculation, analysis and fitting of crystal electric field Hamiltonians, *Journal of Applied Crystallography* **54**, 356 (2021).
- [34] Q. Li, H. Li, J. Zhao, H.-G. Luo, and Z. Y. Xie, Magnetization of the spin- $\frac{1}{2}$  heisenberg antiferromagnet on the triangular lattice, *Phys. Rev. B* **105**, 184418 (2022).
- [35] F. Ferrari and F. Becca, Spectral signatures of fractionalization in the frustrated heisenberg model on the square lattice, *Phys. Rev. B* **98**, 100405 (2018).
- [36] Q. Wang, A. de la Torre, J. A. Rodriguez-Rivera, A. A. Podlesnyak, W. Tian, A. A. Aczel, M. Matsuda, P. J. Ryan, J.-W. Kim, J. G. Rau, and K. W. Plumb, (2024), [arXiv:2407.17559](https://arxiv.org/abs/2407.17559) [cond-mat.str-el].
- [37] P. W. Anderson, Generalizations of the weiss molecular field theory of antiferromagnetism, *Phys. Rev.* **79**, 705 (1950).
- [38] J. Villain, La structure des substances magnetiques, *Journal of Physics and Chemistry of Solids* **11**, 303 (1959).